IJMT. Vol. 22, Iss. 1, 2026. (55-65)

International Journal of Maritime Technology

Journal homepage: ijmt.ir

Vertical Double-Flap Wave Energy Converter: A Novel Concept to Capture Power from Ocean Wave

Hamid Bab[1], Mohammad Mahdi Aziminia[2], Abuzar Abazari[3], Mehdi Behzad[4*]

[1] *Bachelor of Marine Engineering, School of Mechanical Engineering, Sharif University of Technology; hamid.bab@mech.sharif.edu*

[2] *PhD Candidate of Marine Engineering, School of Mechanical Engineering, Sharif University of Technology; mm_aziminia@mech.sharif.edu*

[3] *Associate Professor of Marine Engineering, Chabahar Maritime University, Chabahar, Iran; abuzarabazari@cmu.ac.ir*

[4] *Professor of Mechanical Engineering, School of Mechanical Engineering, Sharif University of Technology; m_behzad@sharif.edu*

ARTICLE INFO

Article History:
Received: 30 Aug 2025
Last modification: 15 Feb 2026
Accepted: 15 Feb 2026
Available online: 17 Feb 2026

Article type:
Research paper

Keywords:
Wave Energy Converter (WEC)
Vertical double flap
Power
Water Wave
Oscillating Wave Surge Converter (OWSC)

ABSTRACT

Wave Energy Converters (WECs) are devices designed to extract electricity from ocean waves. This study introduces a modular flap-type WEC in which a single flap is divided into two vertical segments. This modification aims to investigate its impact on power production. A dynamic model is developed for this dual-flap system, and the governing equations of motion of the system are derived. To account for the interaction between the flaps and the waves, hydrodynamic coefficients and excitation moments are computed using a Boundary Element Method (BEM), which takes the influence of wave-induced forces on each flap into consideration. The rotational motions of both flaps are then analyzed, with an assumption of regular waves. Furthermore, the power generated by each flap is calculated, based on their respective rotational responses. This analysis is aimed to evaluate the efficiency of the dual-flap configuration in harnessing wave energy.

ISSN: 2645-8136

DOI: http://dx.doi.org/10.66224/ijmt.22.1.55

Copyright: © 2026 by the authors. Submitted for possible open access publication under the terms and conditions of the Creative Commons Attribution (CC BY) license [https://creativecommons.org/licenses/by/4.0/]

[Downloaded from ijmt.ir on 2026-10-11]

1. Introduction

As global temperatures continue to rise due to greenhouse gas emissions, the need for low-carbon, sustainable energy alternatives have become increasingly urgent. This has shifted the global focus toward renewable sources that can reduce dependency on fossil fuels and contribute to climate stability. Among the various marine energy forms, wave energy has emerged as a particularly promising candidate. It offers a global theoretical potential ranging between 8,000 and 80,000 TWh per year [1], making it several times greater than other forms of ocean energy such as tidal or thermal gradients. In high-energy coastal regions, wave power densities can reach up to 25 kW/m², making it one of the most energy-rich renewable sources [2].

While global wave energy development has focused on high-energy regions like the Atlantic and Pacific, other areas such as the Persian Gulf and Gulf of Oman also offer localized potential. The Gulf of Oman, in particular, benefits from stronger wave activity and is considered more favorable for wave energy deployment. With appropriate site selection and device optimization, these regions could contribute to regional renewable energy strategies [3].

Various types of wave energy platforms have been developed to harness ocean power, each with unique operating principles. Systems like Pelamis (a multi-body attenuator), point absorbers**,** oscillating water columns**,** and overtopping devices represent the main categories, with designs tailored to specific wave conditions and energy conversion methods. Among these, the Oscillating Wave Surge Converter (OWSC) has gained particular attention for nearshore applications [4]**.** It consists of a bottom-hinged flap attached to the seabed that oscillates. This motion is transferred to a hydraulic Power Take-Off (PTO) system that generates electricity. The OWSC is especially efficient in shallow water**,** where horizontal wave particle velocities are amplified due to wave shoaling, enhancing energy capture.

Mathematical modeling of OWSCs has developed greatly since the work of Cummins [5]**,** who introduced a time-domain formulation where wave radiation forces are expressed through added moment of inertia and convolution terms for radiation damping. This impulse-response function approach became the foundation for modeling wave–structure interaction and has been widely applied to both simple single-degree-of-freedom and more complex multi-degree-of-freedom OWSC systems.

More recently, extended this framework by presenting a methodology for implementing time-domain models of floating structures with multiple motion modes.

Their work demonstrates how frequency-domain hydrodynamic parameters can be transformed into the time domain, enabling realistic simulation of complex, coupled dynamics [6].

The theoretical frameworks developed by Dean and Dalrymple [7] established fundamental principles of wave–structure interaction, while Renzi and Dias [8] provided analytical models specifically designed for OWSC, considering both channel and open-ocean conditions under linear wave theory. These contributions greatly advanced the hydrodynamic analysis of flap-type WECs, offering insight into wave excitation, radiation, and resonance phenomena. Complementing these theoretical developments, large-scale experimental projects such as the Oyster device [9], a surface-piercing, bottom-hinged OWSC deployed off the coast of Orkney, Scotland, have demonstrated the practical feasibility of flap-type converters. The Oyster project validated many aspects of analytical predictions, showing that OWSCs can reliably operate in energetic nearshore environments and confirming their potential as a viable technology for renewable power generation.

Recent studies by Arbabi and Abazari [10] have investigated the influence of flap dimensions, size, and geometric configuration on the power output of wave energy converters. Their findings underscore the importance of geometric optimization in enhancing energy capture efficiency. Furthermore, in another study by Kamal et al. [11], it was demonstrated that flap-type WECs can be effectively integrated with offshore wind turbine platforms, where they contribute to the reduction of structural vibrations. This dual functionality makes flap-type devices particularly promising for application in hybrid offshore energy systems and coastal protection infrastructure.

More recent developments have focused on enhancing energy absorption through segmentation and modularity in flap design. One notable concept was proposed by Lei Zuo et al. [12], who introduced a self-floating OWSC with two vertically stacked segments operating in the water column. In this line, a research work by Abazari et al. [13] investigated a Horizontally segmented OWSC, where a single flap was divided into two segments in horizontal configuration. That study demonstrated that segmentation broadens the frequency response of the device and enhances energy absorption across a wider range of wave periods.

This study proposes a novel configuration of OWSC in which the main flap structure is vertically segmented into two parts—an upper and a lower flap—connected by an internal hinge. Unlike traditional single-body flaps, this arrangement introduces an additional degree of freedom, allowing relative rotation between the segments. As a result, the flap system can adapt more effectively to complex wave profiles. The upper flap, located closer to the free surface, is better positioned to capture energy from the high-energy crest region of waves, where orbital particle motion is strongest [14].

[Downloaded from ijmt.ir on 2026-10-11]

At the same time, the hinged connection enables dynamic interaction between the two segments, improving flexibility.
To assess the performance of this innovative system, the governing equations of motion were derived in the time domain using Lagrangian mechanics. The model was then implemented in ANSYS AQWA to determine the hydrodynamic coefficients of the WEC, including added moment of inertia, radiation damping, and excitation Torques.
Then analysis focused on the rotational response of the upper and lower segments of WEC, also evaluated the power production of this system.

2. Theory

2.1 Dynamic Formulation of Model

In this study, attention is focused on a double flap-type arranged in a vertical modular configuration. The primary flap structure is divided vertically into two segments, an upper and lower flap, which are connected by a mechanical hinge located at the midpoint of the flap height. This configuration introduces an additional degree of freedom compared to conventional single-flap WEC. The system therefore consists of two hinges: the first at the seabed (PTO1), which connects the lower flap to the foundation, and the second at the midpoint (PTO2), The geometry of this configuration is shown in Figure 1, where the two flaps and their associated hinge points are depicted schematically. The lower flap provides absolute rotation with respect to the seabed, while the upper flap rotates relative to the lower segment, together forming a coupled two-degree-of-freedom system.

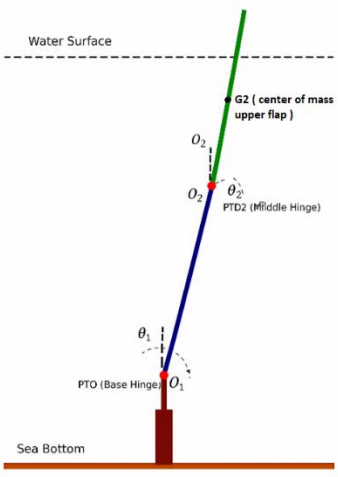

Figure1 Geometry of Double Flap- Horizontal (WEC)

The dynamics of model are modeled using Lagrangian mechanics, considering both rotational kinetic energy and potential energy of system. The system behaves similarly to a inverted double pendulum, where two rotational bodies (flaps) are connected and their motions are strongly coupled.

Lagrangian equations are formulated by summing kinetic and potential energies [15]:

$$K=\frac{1}{2}I_{o1}\dot{\theta_1}^2+\frac{1}{2}m_2V_G^2+\frac{1}{2}I_{G2}\dot{\theta_2}^2 \quad (1)$$

$$V= -m_1g\frac{l_1}{2}(1-\cos\theta_1)-m_2g(l_1(1-\cos(\theta_1)+\frac{l_2}{2}(1-\cos\theta_2)) \quad (2)$$

To evaluate the kinetic energy term in Eq. (1), it is necessary to determine the velocity of the upper flap's center of mass, V_G. By differentiating the position vector of the center of mass with respect to time, the velocity components can be obtained in terms of θ_1, θ_2 and their time derivatives.

Substituting into Eq. (1) leads to nonlinear terms representing both independent and coupled motions of the two flaps. To simplify the expression, the total kinetic energy is reformulated using effective inertia parameters, yielding the compact form:

$$K=\frac{1}{2}J_1\dot{\theta_1}^2+\frac{1}{2}J_2\dot{\theta_2}^2+J_x\dot{\theta_1}\dot{\theta_2}\cos(\theta_2-\theta_1) \quad (3)$$

where the effective inertia terms are defined as:

- $J_1=\frac{m_1l_1^2}{3}+m_2l_2^2$
- $J_2=\frac{m_2l_2^2}{3}$ (4)
- $J_x=\frac{1}{2}m_2l_1l_2$

Here, J_1 represents the combined inertia of the seabed-hinged lower flap and the attached mass of the upper flap. J_2 corresponds to the inertia of the upper flap rotating about its midpoint hinge, while J_x captures the coupling inertia between the two flaps. This compact formulation provides a clear physical interpretation of the energy terms, while preserving the essential nonlinear coupling dynamics of the double-flap system.

The total generalized torque acting at each hinge of the double-flap system is expressed as the sum of several contributions [16]:

$$T(t)=T_{diff}(t)+T_{f-k}(t)+T_{rad}(t)+T_{pto}(t)+T_{vis}(t) \quad (5)$$

where, $T_{diff}(t)$ and $T_{f-k}(t)$, correspond to the diffraction torque and the Froude–Krylov torque, which together represent the external excitation torque produced by the incident wave field. The term $T_{rad}(t)$ accounts for the radiation torque associated with waves generated by the flap motions, while $T_{pto}(t)$ represents the torque due to energy dissipation through the PTO system.

[Downloaded from ijmt.ir on 2026-10-11]

Finally, T_{vis} (t) describes nonlinear viscous damping, which becomes important in capturing additional energy losses caused by flow separation and turbulence around the flaps.

In this model, the effects of subsurface ocean currents are neglected. This assumption is justified by the shallow-water deployment conditions (depths less than 20 meters), where wave-induced forces significantly exceed current-induced forces. This simplification is consistent with standard practice in nearshore OSWEC modeling, as adopted in several foundational and recent studies [12], [13], [16].

From this general decomposition, the torque balance can then be specified separately for the seabed hinge and the internal hinge, giving the corresponding expressions for T_1 (t) and T_2 (t). The hinge-specific torques derived from the generalized Lagrangian formulation can be expressed in a compact vector form, which simultaneously represents the contributions at both the seabed hinge and the internal hinge.

Each hinge torque incorporates the combined effects of wave excitation, added moment of inertia, radiation damping, PTO damping, and viscous damping. These contributions can be systematically expressed in a compact vector form as:

$$\begin{cases} T_1(t) = T_{ext1}(t) - J_{a11}(\infty)\,\theta_1 - J_{a12}(\infty)\ddot{\theta}_2 \\ \sum_{j=1}^{2}\int_{-\infty}^{\tau} K_{1j}(t-\tau)\dot{\theta}_j d\tau - \left(B_{pto1}\right)\dot{\theta}_1 - B_{1v}\dot{\theta}_1|\dot{\theta}_1| \\ T_2(t) = T_{ext2}(t) - J_{a21}(\infty)\ddot{\theta}_1 - J_{a22}(\infty)\ddot{\theta}_2 \\ \sum_{1}^{2}\int_{-\infty}^{\tau} K_{2j}(t-\tau)\dot{\theta}_j d\tau - \left(B_{pto2}\right)\dot{\theta}_2 - B_{2v}\dot{\theta}_2|\dot{\theta}_2| \end{cases} \quad (6)$$

The term J_{aij} represents the added moment of inertia coefficient in the hydrodynamic model. It quantifies the extra inertia that the fluid adds to flap i due to the acceleration of flap j. When i=j is the added moment of inertia of a flap caused by its own acceleration, and when i≠j, it reflects the coupling effect between the two flaps. Similarly, the radiation damping $K_{ij}(t-\tau)$ describes the time-dependent damping forces due to waves radiated by degrees j acting on flap i. It is calculated from the frequency-dependent radiation damping coefficients $B_{ij}(\omega)$ by the integral [5]:

$$K_{ij}(t-\tau) = \frac{2}{\pi}\int_0^{\infty} B_{ij}(\omega)\cos(\omega t)d\omega \quad (7)$$

This formulation originates from Cummins' equation, which provides the time-domain representation of wave–structure interaction. In this framework, the convolution integral with kernel $K_{ij}(t-\tau)$ captures the radiation memory effect, allowing the present model to account for both self-radiation and cross-radiation coupling between the two flaps.

The coupled nonlinear equations of motion, obtained through the Lagrangian formulation, are expressed with i indexing the components and j indexing the degrees of freedom:

$$\begin{cases} \left(J_1 + J_{a11}(\infty)\right)\ddot{\theta}_1(t) + \left(J_{a12}(\infty)\right)\ddot{\theta}_2(t) + (J_x)\cos(\theta_1-\theta_2)\ddot{\theta}_2(t) \\ +\sum_{j=1}^{2}\int_{-\infty}^{\tau} K_{1j}(t-\tau)\dot{\theta}_j d\tau + \left(B_{pto1}\right)\dot{\theta}_1 + B_{1v}\dot{\theta}_1(t)|\dot{\theta}_1(t)| \\ +(J_x)\dot{\theta}_2(t)^2\sin(\theta_1-\theta_2) + C_1\theta 1 + 2C_2\theta 2 = T_{1ext}(t) \\ \left(J_2 + J_{a22}(\infty)\right)\ddot{\theta}_2(t) + J_{a21}(\infty)\ddot{\theta}_1(t) + (J_x)\cos(\theta_1-\theta_2)\ddot{\theta}_1(t) \\ +\sum_{1}^{2}\int_{-\infty}^{\tau} K_{2j}(t-\tau)\dot{\theta}_j d\tau + \left(B_{pto2}\right)\dot{\theta}_2(t) + B_{2v}\dot{\theta}_2(t)|\dot{\theta}_2(t)| \\ -(J_x)\dot{\theta}_1(t)^2\sin(\theta_1-\theta_2) + (C_2)\theta_2 = T_{2ext}(t) \end{cases} \quad (8)$$

In Eq. (8), the terms C_1 and C_2 denote the hydrostatic restoring stiffness of the upper and lower flaps. These coefficients are obtained directly from the flap dimensions [16]:

$$C_{\text{hyrostatic restoring}} = \frac{(1-\alpha)}{2}\rho_w g t W L^2 \quad (9)$$

Where α is the ratio of plate density ρ_p to water density ρ_w, g the gravitational acceleration, and t, W, and L are the flap thickness, width, and length, respectively.

However, by assuming small-amplitude rotation and neglecting viscous effect, which has only a minor effect at small angular displacements [17], the coupled nonlinear equations of motion in Eq. (8) can be linearized. This simplification allows the system to be expressed in a linear form, the system can be:

$$\begin{cases} \left(J_1 + I_{a11}(\infty)\right)\ddot{\theta}_1 + \left(J_x + I_{a12}(\infty)\right)\ddot{\theta}_2 + \int_{-\infty}^{\tau} K_{11}(t-\tau)\dot{\theta}_1 d\tau \\ +\int_{-\infty}^{\tau} K_{12}(t-\tau)\dot{\theta}_2 d\tau + \left(B_{pto1}\right)\dot{\theta}_1 + C_1\theta_1 + 2C_2\theta_2 = T_{1ext}(t) \\ \left(J_x + I_{a21}(\infty)\right)\ddot{\theta}_1 + \left(J_2 + I_{a22}(\infty)\right)\ddot{\theta}_2 + \int_{-\infty}^{\tau} K_{21}(t-\tau)\dot{\theta}_1 d\tau \\ +\int_{-\infty}^{\tau} K_{22}(t-\tau)\dot{\theta}_2 d\tau + \left(B_{pto2}\right)\dot{\theta}_2 + (C_2)\theta_2 = T_{2ext}(t) \end{cases} \quad (10)$$

2.2 Power Frequency Response

Since this methodology relies on linear wave theory, it is assumed that the response amplitudes remain small. Thus, for accurate predictions, angular displacements exceeding 30° are excluded, as the system assumes small-amplitude waves for its analysis.

The time-domain formulation of power dissipation due to linear PTO damping is:

$$P(t) = T \times V = B_{pto}\dot{\theta}(t)^2 \quad (11)$$

Assuming harmonic motion with the form of $\boldsymbol{\theta(t) = |\Theta|\sin(\omega t + \emptyset)}$, the average power extracted during a complete rotation cycle is expressed as in [16], [18]. The power expression can be derived by integrating the dissipated energy due to rotational damping over a full period and simplifying it in the frequency domain, as

[Downloaded from ijmt.ir on 2026-10-11]

follows which the fully derivation of this equation is obtained and reported in Appendix A:

$$\overline{P} = \frac{1}{T}\int_0^T B_{pto}\dot{\theta}(t)^2\,dt = \frac{1}{2}\omega^2 B_{pto}|\Theta|^2 \tag{12}$$

From Eq. (12), for the model with two flaps, the total power extracted consists of two components: one from the motion of Flap 1, and the other from the relative motion between Flap 2 and Flap 1. Thus, the total average power in the frequency domain is given by:

$$\overline{P_{totall}(\omega)} = \overline{P_1(\omega)} + \overline{P_2(\omega)} = \frac{1}{2}\omega^2 B_{pto1}|\theta_1(\omega)|^2 + \frac{1}{2}\omega^2 B_{pto2}|\theta_2(\omega) - \theta_1(\omega)|^2 \tag{13}$$

The hydrodynamic coefficients—such as added moment of inertia, radiation damping, and excitation moment—are typically complex and cannot be accurately derived using analytical methods. These coefficients can be obtained through numerical approaches such as Computational Fluid Dynamics or Boundary Element Methods (BEM), both of which are commonly used in marine hydrodynamics. In this study, the BEM-based software ANSYS AQWA is employed to compute these parameters.

2.3 Potential Flow Theory and BEM for Wave Energy

The potential flow theory is commonly used to assess the hydrodynamic interaction between waves and structures, assuming inviscid**,** irrotational, and incompressible flow. This allows for the existence of a velocity potential Φ, which satisfies the governing Laplace equation for mass conservation [8] , [19]:

$$\nabla^2\Phi = \nabla^2 R[(\Phi_I + \Phi_R + \Phi_D)] = 0 \tag{14}$$

In the context of WEC, the total wave potential is the sum of three key components: the incident wave potential Φ_I represents the incoming wave field, which interacts with the structure, causing rotation.

The incident wave potential Φ_I for a bottom-hinged flap is given by the following expression [20]:

$$\Phi_I = \frac{H}{2}\frac{g\cosh(k(d+z)}{\omega\cosh(kd)}\sin(kx - \omega t) \tag{15}$$

where H is the wave height, k is the wave number, d is the water depth, z is the vertical position, ω is the wave frequency, x is the horizontal position, and t is time.

Eq. (15) describing the incoming wave field that interacts with the structure. At large depths, the wave potential is found to tend to zero, indicating that no wave effects are present at that location. On the other hand, when z is very small (close to the surface), the wave potential's velocity and acceleration are maximized. This theory is applied to model the dynamics of the flap, as it is capable of accurately capturing the wave-induced forces and interactions near the surface.

The radiation wave potential Φ_R accounts for the waves generated by the oscillating structure itself, reflecting the interaction of the structure with the surrounding fluid.

Finally, the diffraction wave potential Φ_D describes the diffraction of the incident waves caused by the presence of the structure, which disturbs the wave propagation. These potentials collectively describe the fluid-structure interaction in wave energy conversion and are critical for calculating the forces acting on the WEC.

In ANSYS AQWA, BEM is an efficient numerical method for solving potential flow problems. BEM discretizes the boundaries of the structure into a mesh of nodes and elements, typically using triangular or quadrilateral elements. The fluid's behavior is determined by applying boundary conditions, such as wave elevation and particle velocity, to these nodes.
The system of equations derived from the potential flow problem is then solved to calculate key hydrodynamic coefficients [21]. This approach is computationally efficient as it reduces the problem to surface integrals.

3. Validation

A critical step in validating the present numerical method is the accurate computation of hydrodynamic parameters includes added moment of inertia, radiation damping and wave excitation torque.

The numerical model developed in this study was built upon a well-established validation chain. Van Hoff [22] conducted experimental tests on a single flap-type wave energy converter, providing benchmark data for hydrodynamic performance. Subsequently, Renzi and Díaz [20] developed advanced semi-analytical methods to model a single-flap WEC and validated their results against Van Hoff's experimental data, demonstrating good agreement for key hydrodynamic coefficients.

[Downloaded from ijmt.ir on 2026-10-11]

In this study, a single rigid flap was modeled in ANSYS AQWA using the BEM approach, and the results were found to be consistent with the findings of Renzi and Díaz [20], confirming the reliability of the modeling process which is shown in the following.

The geometric characteristics of the single flap, along with the wave conditions applied in the numerical model are summarized in Table 1. Also, A visual representation of the modeled flap geometry is shown in Figure 2.

Table 1. Characteristics of a Single WEC for the numerical model

Characteristic	Value
Height	9 m
Width	18 m
Thickness	1.8 m
Density	250 $\frac{kg}{m^3}$
Foundation height	1.8 m
Mass	74,722 kg
Water Depth	10.9 m
Incident wave amplitude	0.30 m

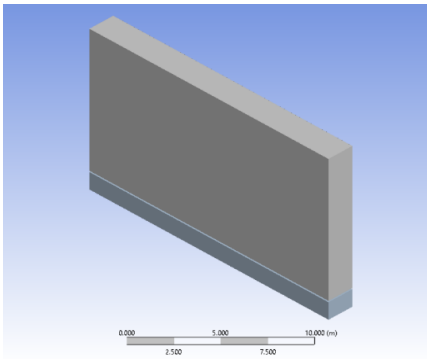

Figure 2. Numerical model of the Single WEC modeled in ANSYS AQWA

Figures 3, 4, and 5 show the variation of the added moment of inertia, radiation damping, and excitation moment as functions of wave period. As shown in the plots, the hydrodynamic coefficients were obtained through ANSYS AQWA exhibit strong agreement with the semi-analytical results reported by Renzi and Díaz [20], thereby confirming the validity of the numerical approach. Minor discrepancies between the two methods have been observed, due to differences in modeling assumptions. In the AQWA simulations, the flap was modeled as a submerged body, whereas in the Renzi–Díaz model, it was considered as a surface-piercing structure. This difference in boundary conditions can slightly influence the resulting hydrodynamic response.

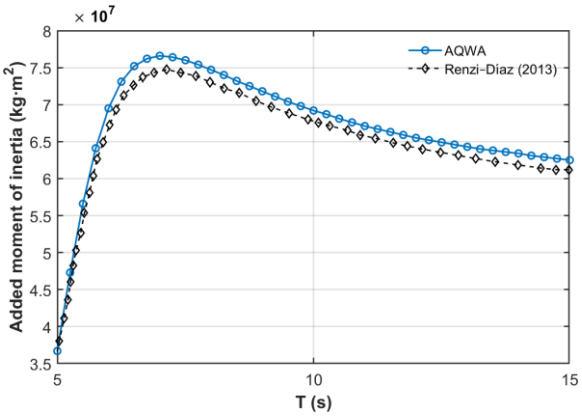

Figure 3. Added moment of inertia coefficient for Single WEC (this study and reference [20]))

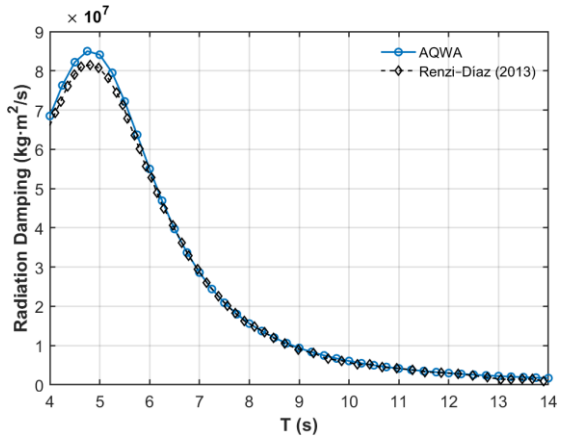

Figure 4. Radiation damping coefficient for single WEC(this study and reference [20]))

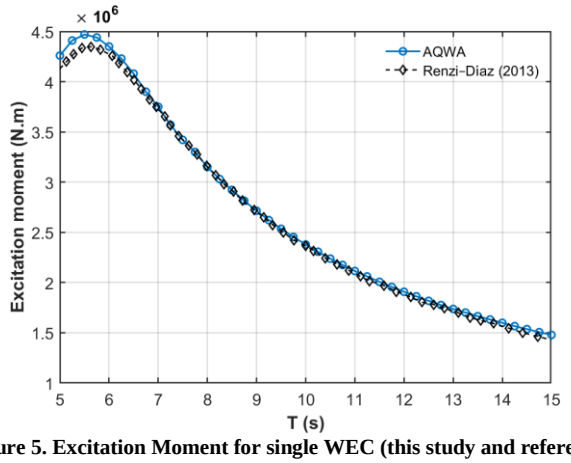

Figure 5. Excitation Moment for single WEC (this study and reference [20]))

Based on the validated numerical method established in this work, a new vertical double-flap configuration has been analyzed. Although no direct experimental data are available for this configuration that is an innovative concept. However, a related study involving a self-floating wave energy converter is reference [12] which employs a dynamic formulation similar to this study in Eq. (10). While that system is floating and the

[Downloaded from ijmt.ir on 2026-10-11]

present model is bottom-fixed, the mathematical structure and general dynamic behavior are comparable. Therefore, the present numerical model- developed using ANSYS AQWA and BEM- can be considered reliable for analyzing the hydrodynamic performance of the proposed double-flap wave energy converter.

4. Results and Discussion

Based on the conceptual design of the flap-type wave energy converter, the Vertical Double-Flap WEC is constructed by dividing a single flap into two vertically aligned segments. The geometric characteristics of this double-flap configuration are identical to those of the single-flap system, with the exception that each segment has a height of 4.5 m and a mass of 37,361 kg, as summarized in Table 1. Similar to single flap analysis as shown in the Table 1, incident wave amplitude is assumed 0.3 m here. The upper and lower flap segments are identical and mechanically linked to operate as a single articulated structure, which are mounted on a base rigidly fixed to the seabed.

The Vertical Double Flap WEC geometry was modeled in ANSYS AQWA. The model was used to calculate the hydrodynamic coefficients and the flap displacements under wave excitation, which were further employed to estimate the power production of the system. A representative view of the numerical model is shown in Figure 6.

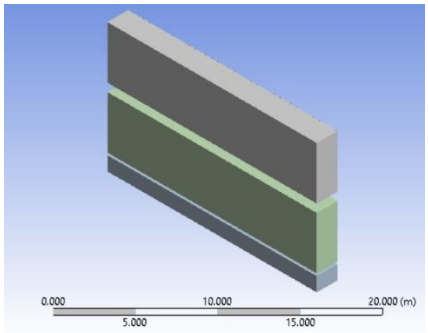

Figure 6. Numerical model of the Vertical Double Flap WEC in ANSYS AQWA

4.1 Mesh Analysis

A mesh analysis was conducted using ANSYS AQWA to evaluate the impact of mesh resolution on the hydrodynamic coefficients computed by the BEM. Three mesh sizes were tested: 0.3 m, 0.25 m, and 0.2 m.

A representation of the mesh used in the simulation is shown in Figure 7, illustrating the discretization of the structure's boundaries and the application of boundary conditions.

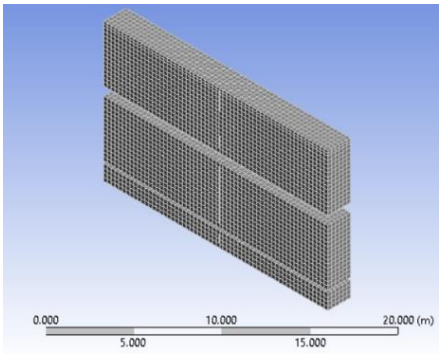

Figure 7. Mesh of the Double Flap

The results showed that the 0.3 m mesh provided a good trade-off between computational efficiency and accuracy, with negligible relative errors in the added moment of inertia compared to finer meshes. Table 2 presents the added moment of inertia of the upper flap for different encounter periods, along with the corresponding relative errors. To evaluate the influence of mesh size on the numerical results, a mesh sensitivity analysis was conducted by comparing the added moment of inertia values obtained from different mesh resolutions. The relative error for each mesh size was calculated with reference to the results from the 0.3 m mesh, which was selected as the baseline. As presented in Table 2, the differences across mesh sizes are all below 0.5 %, indicating excellent convergence and minimal sensitivity to further refinement. Based on these findings, the 0.3 m mesh is selected for all final simulations, ensuring mesh-independent results while minimizing computational cost.

Table 2. Mesh sensitivity analysis: Added Moment of inertia of the upper flap

Mesh Size(m) / Encounter Period (s)	0.3 Added moment of Inertia (kg· m^2) - Reference	0.25 (% error)	0.2 (% error)
3	3126.10	-0.11%	-0.41%
8	5751.07	+0.22%	+0.29%
12	5242.35	+0.17%	+0.20%
15	5114.39	+0.15%	+0.19%
20	5021.51	+0.15%	+0.20%

Radiation damping and excitation moments showed similar convergence behavior, with differences under 1%.

As shown in Figure 8, the added moment of inertia of the lower flap exhibits very similar trends for all assumed mesh sizes over the considered wave periods, with only minor deviations observed, indicating a weak sensitivity of the results to further mesh refinement. This suggests that using finer meshes would offer negligible improvement in accuracy while significantly increasing computational cost.

[Downloaded from ijmt.ir on 2026-10-11]

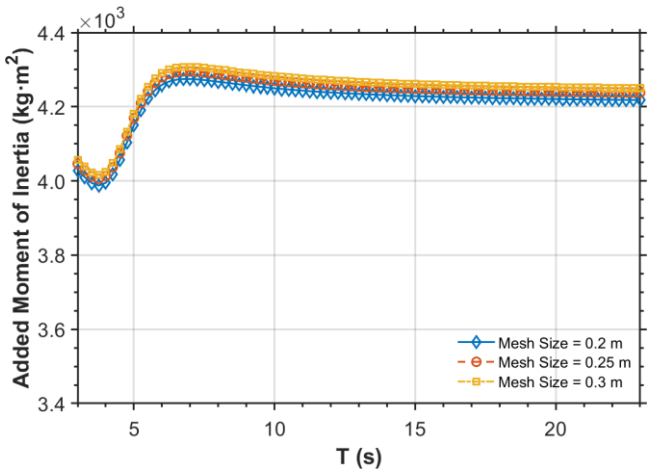

Figure 8. Mesh sensitivity analysis of the added moment of inertia of the lower flap as a function of wave period.

4.2 Hydrodynamic Coefficients

Hydrodynamic coefficients are calculated to quantify the interaction between waves and the flaps of the Vertical Double Flap WEC. They provide essential information on how the surrounding fluid affects the motion of the device, including the forces it experiences and the energy it can extract from waves. In this study, the differences in hydrodynamic behavior between the upper and lower flap segments are also analyzed to assess their individual contributions to the overall performance.

4.2.1 Added Moment of Inertia

As shown in Figure 9, the added moment of inertia of both the lower and upper flaps of the Vertical Double Flap WEC was obtained from the numerical simulations.

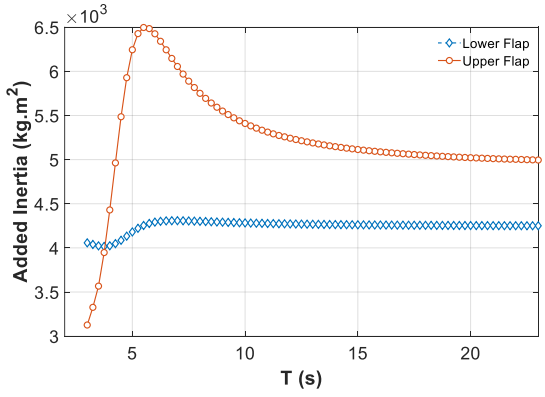

Figure 9. Added moment of inertia coefficient for Vertical Double WEC

The results indicate that the upper flap exhibits significantly higher added moment of inertia than the lower flap across the wave periods, this difference arises because wave-induced particle accelerations are larger near the free surface, where fluid particles move more freely. In contrast, the lower flap is closer to the seabed, where fluid motion is constrained, resulting in lower added moment of inertia. Consequently, the upper flap, being near the surface, experiences significantly higher added moment of inertia than the lower flap.

Furthermore, at high frequencies, the added moment of inertia of each flap approaches a constant value. This occurs because the fluid's response becomes dominated by local inertia, and the pressure distribution around the flap stabilizes, making the added moment of inertia nearly frequency-independent.

4.2.2 Radiation Damping

Radiation damping quantifies the energy lost by the WEC due to waves radiated away as a result of its motion. It represents the dissipative component of the hydrodynamic interaction, the portion of energy that cannot be recovered because it propagates away as outgoing waves. In the present study, as shown in Figure 10, the numerical results indicate that the Upper Flap exhibits higher radiation damping than the lower Flap across the range of wave periods considered.

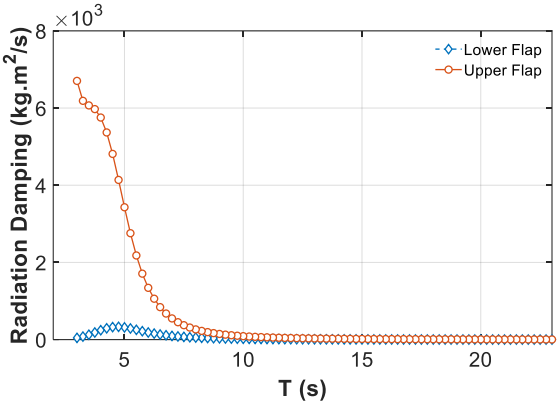

Figure 10. Radiation damping coefficient for Vertical Double WEC

The Upper Flap exhibits higher radiation damping than the lower Flap due to its proximity to the free wave surface, where wave-induced pressures and particle velocities are larger. The lower Flap, being deeper, experiences reduced wave energy. Radiation damping reflects the energy lost as waves radiated away by the flap motion; the upper Flap, generating stronger outgoing waves, loses more energy to the fluid, while the lower Flap interacts with weaker wave motions.

[Downloaded from ijmt.ir on 2026-10-11]

Overall, this indicates that the upper Flap is more effective in interacting with incident waves and contributes more significantly to the energy extraction of the wave energy converter system.

4.2.3 Excitation Moment

The excitation moment represents the torque applied to each flap due to the incident wave forces, which arise from the Froude-Krylov and diffraction moments of the wave. Figure 11 illustrates the excitation torque for both the upper and lower flaps. It is evident that the upper flap experiences a higher excitation torque compared to the lower flap.

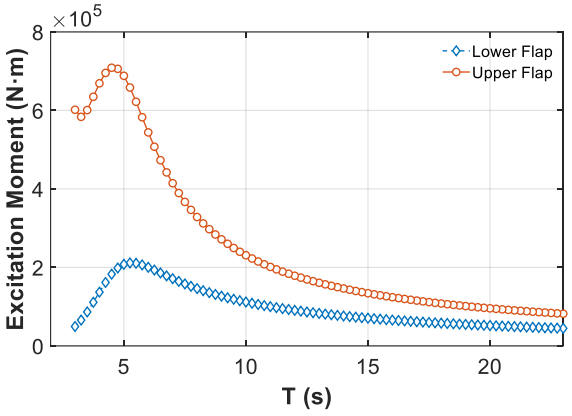

Figure 11. Excitation Moment applied on Vertical Double WEC

The higher excitation torque on the upper Flap arises from the greater wave-induced forces near the water surface, where particle velocities and pressures are stronger. This results in a larger integral of hydrodynamic forces acting on the flap, producing a stronger rotational moment.

4.3 Rotational Displacement Response

As shown in Figure 12, the model in ANSYS AQWA is analyzed under a regular wave. The damping values for the lower and upper PTOs are 300,000 N·m(°/s) and 30,000 N·m(°/s) , respectively. These damping values are chosen to ensure model stability, with the upper part experiencing more rotation and thus requiring lower damping. Figure 13 shows the rotational response of the upper and lower Flaps over time under regular wave excitation. The upper Flap, exhibits larger motion compared to the lower Flap. This difference is consistent with the hydrodynamic characteristics discussed earlier. The response is shown for a duration of 0 to 1000 s, providing insight into both transient and steady-state behavior.

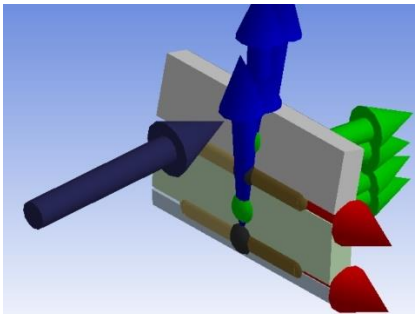

Figure 12. Motion of Vertical Double WEC in AQWA

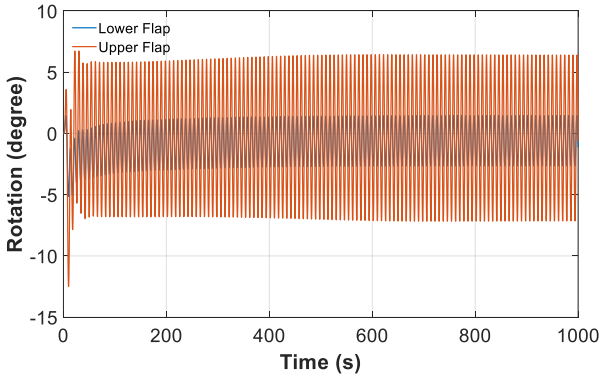

Figure 13. Rotational Displacement Response in A=0.3m,T=8s

As in Figure 14, the maximum rotation of the model per period is calculated. As shown in this figure, the upper flap exhibits a larger rotation, consistent with the predictions.

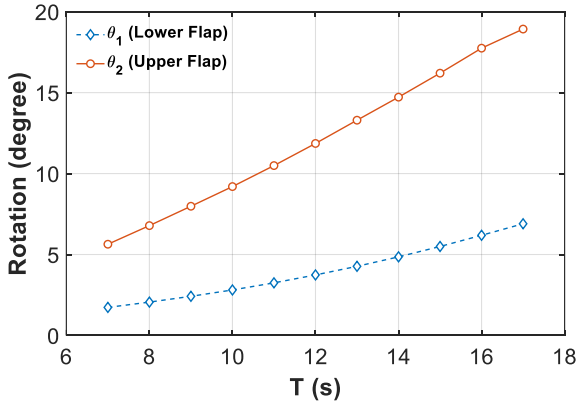

Figure 14. Rotation per Wave Period in A=0.3m

4.4 Power Production

Figure 15 shows the power production per period for A = 0.3, calculated using Eq. (13). The calculation is based on the rotational motions of both the upper and lower flaps obtained in Section 4.3. Specifically, the contribution of each flap to the total power production is determined from its maximum rotational amplitude: the upper flap exhibits higher rotation, resulting in a larger share of generated power, while the lower flap has smaller rotations and contributes less. The analysis presented here does not account for the effect of optimum damping.

[Downloaded from ijmt.ir on 2026-10-11]

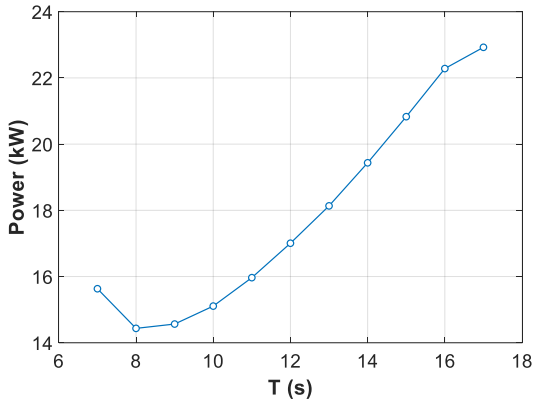

Figure 15. Power Production per Wave Period in A=0.3m

4. Conclusions

In the present work, a novel Wave Energy Converter model consisting of two vertically split segments is introduced, and its effect on power production is investigated. The governing equations for each flap are derived to describe their dynamic behavior under wave excitation. Hydrodynamic coefficients and excitation moments are obtained using the Boundary Element Method, which captures the interactions between the flaps and the surrounding water.

Due to higher accelerations near the water surface, the upper flap experiences greater radiation damping, added moment of inertia, and torque compared to the lower flap. These differences in hydrodynamic response lead to distinct rotational behaviors for each flap under the same wave conditions. Numerical simulations are performed to calculate the rotational motion of each flap over a range of wave periods. The results indicate that the upper flap exhibits larger rotations than the lower flap, consistent with the predictions based on surface wave effects. Using these rotational motions, the power production of the WEC is calculated, showing the contribution of both segments to the total energy output.

This work introduces a new concept in wave energy converters, focusing on the dynamic behavior of a two-segment model. The primary emphasis here is not on power production, In the next step, the power optimization of this model can be explored to improve its efficiency and overall energy output.

Appendix A

Using harmonic motion with the form of $\theta(t) = |\Theta|\sin(\omega t + \emptyset)$ **; hence,** $\dot{\theta}(t) = |\Theta|^2\omega^2\cos^2(\omega t + \emptyset)$ **, also**

$$\overline{P} = \frac{1}{T}\int_0^T B_{pto}\dot{\theta}(t)^2\,dt = \frac{1}{T}\int_0^T B_{pto}\omega^2|\theta|^2\cos^2(\omega t + \varphi)\,dt$$
$$= \frac{B_{pto}\omega^2|\theta|^2}{T}\int_0^T \cos^2(\omega t + \varphi)\,dt$$

The abovementioned integral is obtained:

$$\int_0^T \cos^2(\omega t + \varphi)\,dt \overset{\omega=\frac{2\pi}{T}}{=} \int_0^T \cos^2\left(\frac{2\pi}{T}t + \varphi\right)dt$$

$$= \frac{T\sin\left(2\left(\frac{4\pi t}{T}\right)+\emptyset\right)+8\pi t}{16\pi} + C\Big|_0^T = \frac{T\sin(2\emptyset)+2T\emptyset+8\pi t}{16\pi} - \frac{T\sin(2\emptyset)+2T\emptyset}{16\pi} =$$

$$\frac{(8\pi)T}{(16\pi)} = \frac{T}{2}$$

Using this relation, the power production formulation is derived as :

$$\overline{P} = \frac{1}{T}\int_0^T B_{pto}\dot{\theta}(t)^2\,dt = \frac{B_{pto}\omega^2|\theta|^2}{T}\int_0^T \cos^2(\omega t + \varphi)\,dt =$$
$$\frac{B_{pto}\omega^2|\theta|^2}{T} \times \frac{T}{2} = \frac{1}{2}\omega^2 B_{pto}|\Theta|^2$$

5. References

1- IEA-OES, *IEA-OES Annual Report*, Technical Report, International Energy Agency – Ocean Energy Systems, 2007.

2- B. Czech and P. Bauer, "Wave energy converter concepts: Design challenges and classification," *IEEE Industrial Electronics Magazine*, vol. 6, no. 2, pp. 4–16, 2012. https://doi.org/10.1109/MIE.2012.2193290

3- A. Shafieefar and B. Kamranzad, "A Review of Tidal and Wave Energy in Southern Waters of Iran," *Journal of Marine Science*, vol. 2, no. 3, pp. 21-27, 2011.

4- A. F. de O. Falcão, "Wave energy utilization: A review of the technologies," *Renewable and Sustainable Energy Reviews*, vol. 14, no. 3, pp. 899–918, 2010. https://doi.org/10.1016/j.rser.2009.11.003

5- W. L. Cummins, *The impulse-response function and ship motions*, Aeronautics and Astronautics, presented at the Symposium on Ship Theory, Institute für Schiffbau der Universität Hamburg, Hamburg, Germany, Jan. 25–27, 1962.

6- W. Sheng, E. Tapoglou, X. Ma, C. J. Taylor, R. Dorrell, D. R. Parsons, and G. Aggidis, "Time-domain implementation and analyses of multi-motion modes of floating structures," *Journal of Marine Science and Engineering*, vol. 10, no. 5, p. 662, 2022. https://doi.org/10.3390/jmse10050662

7- R. G. Dean and R. A. Dalrymple, *Water Wave Mechanics for Engineers and Scientists*. World Scientific, 1991. https://doi.org/10.1142/1232

[Downloaded from ijmt.ir on 2026-10-11]

8- E. Renzi and F. Dias, "Relations for a periodic array of flap-type wave energy converters," *Applied Ocean Research*, vol. 39, pp. 31–39, 2012. https://doi.org/10.1016/j.apor.2012.09.002

9- *The Oyster: World's first nearshore wave energy converter*, London Research International, 2013.

10. E. Arbabi and A. Abazari, "The effects of dimension, geometry and the modules' orientation in a modular flap arrangement on the extracted power density of surge oscillating flap wave energy converter," Journal of Marine Engineering, vol. 14, pp. 14–25, 2020.

https://doi.org/10.61186/marineeng.19.41.14

11. F. Kamal, A. Abazari, and R. Dorostkar, "The effect of flap dimension and wave angle on the dynamic response and extracted power of the hybrid system of offshore wind turbine and surge oscillating converter," Journal of Marine Engineering, vol. 20, no. 42, pp. 1–12, 2023. https://doi.org/10.61186/marineeng.20.42.1

12- Q. Li, J. Mi, X. Li, S. Chen, B. Jiang, and L. Zuo, "A self-floating oscillating surge wave energy converter," *Applied Energy*, vol. 257, p. 114031, 2020. https://doi.org/10.1016/j.energy.2021.120668

13- A. Abazari, & M.M Aziminia, (2022). *Enhanced power extraction by splitting a single flap-type wave energy converter into a double configuration*. Renewable Energy Research and Application (RERA), 4(2), 243–249. https://doi.org/10.22044/rera.2022.11846.1118

14- M. Faizal, M. R. Ahmed, and Y.-H. Lee, "On utilizing the orbital motion in water waves to drive a Savonius rotor," *Renewable Energy*, vol. 34, no. 5, pp. 1084–1092, 2009. https://doi.org/10.1016/j.renene.2009.03.015

15- Tan, Z. (2022). Investigation of the double pendulum small angle approximation model. *World Scientific Research Journal*, *8*(11), 342-352. https://doi.org/10.6911/WSRJ.202211_8(11).0042

16- Gomes, R. P. F., Lopes, M. F. P., Henriques, J. C. C., Gato, L. M. C., & Falcão, A. F. O. (2015). The dynamics and power extraction of bottom-hinged plate wave energy converters in regular and irregular waves. *Ocean Engineering*, *92*, 922-934. https://doi.org/10.1016/j.oceaneng.2014.12.024

17- J. Falnes, *Ocean Waves and Oscillating Systems: Linear Interactions Including Wave-Energy Extraction*. Cambridge, UK: Cambridge University Press, 2002.

https://doi.org/10.1017/9781108674812

18- Abazari, A., and Aziminia, M. M., "Water wave power extraction by a floating surge oscillating WEC comprising hinged vertical and horizontal flaps," Journal of Energy Management and Technology, 2022. https://doi.org/10.22109/jemt.2022.345654.1391

19- He, C., Zhou, L., & Ma, X. (2023). Hydrodynamic response of a large-scale mariculture ship based on potential flow theory. *Journal of Marine Science and Engineering*, *11*(10), 1995. https://doi.org/10.3390/jmse11101995

20- Renzi, E., & Dias, F. (2013). Hydrodynamics of the oscillating wave surge converter in the open ocean. *European Journal of Mechanics - B/Fluids*, *39*, 1-11. https://doi.org/10.1016/j.euromechflu.2013.01.007

21- Raghavan, V., Lavidas, G., Metrikine, A., Mantadakis, N., & Loukogeorgaki, E. (2023). A comparative study on BEM solvers for wave energy converters. In *Proceedings of the 2023 International Conference on Wave Energy (ICWE)* (pp. 391–398). CRC Press. https://doi.org/10.1201/9781003360773-50

22- M. Folley, T. W. T. Whittaker, and J. van't Hoff, "The design of small seabed-mounted bottom-hinged wave energy converters," in Proceedings of the 7th European Wave and Tidal Energy Conference (EWTEC), Porto, Portugal, 2007.

[Downloaded from ijmt.ir on 2026-10-11]